



Integrated Geophysical and Hydrogeological Approaches for Aquifer Characterization in the Northeast part of Menoua Division in Cameroon



Jean Victor Kenfack^{*}, Rodrigue Talla Toteu^{}, Malick Rosvelt Demanou Messe^{}, Stéphane Tchomtchoua Tagne^{}, Rosvaltine Kune Emshie Rosvaltine^{}, Lucas Kengni^{}

Laboratory of Environmental Geology, Department of Earth Sciences, University of Dschang, P.O. Box 67 Dschang, Cameroon

* Correspondence: Jean Victor Kenfack (victor.kenfack@univ-dschang.org)

Received: 09-25-2025

Revised: 11-30-2025

Accepted: 12-08-2025

Citation: J. V. Kenfack, R. Talla Toteu, M. R. Demanou Messe, S. Tchomtchoua Tagne, R. Kune Emshie Rosvaltine, and L. Kengni, "Integrated geophysical and hydrogeological approaches for aquifer characterization in the northeast part of Menoua Division in Cameroon," *J. Civ. Hydraul. Eng.*, vol. 3, no. 4, pp. 212–230, 2025. <https://doi.org/10.56578/jche030404>.



© 2025 by the author(s). Licensee Acadlore Publishing Services Limited, Hong Kong. This article can be downloaded for free, and reused and quoted with a citation of the original published version, under the CC BY 4.0 license.

Abstract: The primary goal of this research was to delineate optimal zones for the establishment of wells by integrating geophysical and hydrogeological techniques, namely electrical resistivity tomography and piezometric analysis. Carried out on the southern flank of Mount Bamboutos within the Menoua Division in Cameroon, the current study addressed the local issue of inadequate water supply, which persists in view of the scarcity of water resources and limited success achieved by previous initiatives. A total of 21 wells and 31 Vertical Electrical Sounding (VES) locations were investigated and seven distinct geophysical anomalies were identified, with resistivity values ranging from 28.61 to 216 703 Ω·m, and thicknesses varying from 0.228 to 46.64 meters. The anomalies were associated with weathered geological formations, including decomposed rocks, fractured basaltic trachytes, and alteritic layers. Considerable spatial variations were found in hydraulic parameters: (i) Hydraulic conductivity ranged between 0.004 and 16.915 m/day; (ii) Transmissivity values extended from 0.017 to 227.841 m²/day; and (iii) Porosity estimates fluctuated between 0.736% and 38.226%. Aquifers hosted in alteritic materials were found at depths about 1.63 to 26 m whereas those associated with fractured basaltic trachytes exceeded 26 m in depth. Piezometric measurements revealed a predominant groundwater flow direction from the northeast toward the southwest. Depressed hydraulic head zones, particularly in the southwestern and central areas, were considered favorable for groundwater exploitation. Aquifer thicknesses ranged from 14.7 to 46.6 m primarily concentrated in the southwestern, southeastern, central, and northern parts of the study area. Based on the integration of geophysical and piezometric data, a hydrogeological map was generated to highlight several promising zones for borehole development. The map serves as a practical decision-support tool to select favorable drilling sites, reduce borehole failure rates and directly support the planning of local water supply. The outcome of this multidisciplinary investigation provided valuable contributions to guide the sustainable management and development of groundwater resources in the region.

Keywords: Menoua Division; 1D and 2D electrical tomography; Piezometry; Aquifers; Hydraulic parameters; Hydrogeological map

1 Introduction

Water, representing one of the most basic necessities of life, plays a critical role in sustaining ecosystems and human well-being. As global population and economic activities expand, there is a considerable increase in the demand for water. Many parts of the world are, however, experiencing significant water shortages, leading to an alarming situation which inhabitants should be highly conscious and attentive, so better conservation of resources, in particular water resources, is urgently required [1]. Over the last century, global water consumption has multiplied sixfold [2] and continues to rise as a result of unchecked urban development; for many Africans, access to reliable water distribution networks remains to be limited. In general, human consumption of water primarily relies on either surface water or groundwater derived from aquifers. Groundwater, which resides beneath the Earth's surface inside soil pores and fractured rock formations [3], accounts for approximately 98% to 99% of the terrestrial soft

water [4]. Due to limited accessibility, groundwater is less vulnerable to contamination and relatively well-protected from sources of pollution such as animal activities [5]. The Menoua Division is a specific case where several sources of surface water are subject to risks of contamination from agricultural runoff like fertilizers and pesticides, untreated domestic wastewater, and livestock activities. Previous studies in the western highlands reported elevated concentrations of nitrates and coliform bacteria in streams though boreholes and hand-dug wells generally met the standards of drinking water stipulated by the World Health Organization (WHO). This background highlighted the importance of groundwater as a comparatively safer and more reliable resource for the local population. Cameroon is no exception to this situation, despite numerous hydraulic projects implemented in both rural and urban areas.

Although Cameroon is abundant in water resources, with approximately 120 billion m³ of usable groundwater resources, its distribution is unevenly spread [6]. In many rural areas of Cameroon such as the Nord-Est region of the Menoua Division, water supply is primarily reliant on hand-dug wells and boreholes aimed at locating sources of groundwater that generally meet the standards of the WHO in terms of quality [7]. Unfortunately, the access of groundwater in Cameroon remains to be limited. To ensure proper management and utilization of underground water, it is necessary to conduct geological, hydrogeological, and geophysical surveys, which provide invaluable knowledge regarding the geometric, electrical, and hydrodynamic characteristics of aquifers to serve as a guide for siting various hydraulic structures [8–10]. In hydrogeology, various techniques including electrical methods and remote sensing are vital for accurately identifying and describing aquifers, in order to support effective groundwater development strategies. These methods help to identify areas with high groundwater potential and determine suitable locations for the installation of hand-dug wells and boreholes, thus improving the water conditions and access for the population [11, 12].

The access to safe drinking water remains a significant challenge in various regions of Cameroon, largely due to factors such as high population pressure, inadequate investment in the water sector, and the impacts of climate change. This unfortunate situation leaves approximately 70% to 80% of the towns in Cameroon running without access to reliable water sources [13]. The problem of inadequate water supply is even more severe in rural areas where the majority of population relies heavily on both ground and surface water to meet their basic needs [14]. To address the problem of water accessibility, numerous well and borehole projects have been implemented. However, these projects faced significant failure rates, which lead to social and financial complications. It is therefore imperative to exercise caution in the selection and placement of hydraulic structures such as wells and boreholes, in order to ensure that they are situated in favorable zones. The population in the study area is particularly affected by these challenges as a significant portion of the community relies on underground water resources for their daily activities. Nevertheless, several wells in the area have dried up, and others have been abandoned due to various reasons. Either the true water accumulation zones were not accurately identified in the areas with dried-up wells, or the wells were constructed in unfavorable locations due to a lack of knowledge regarding the geophysics and hydrogeology of the area. Consequently, some residents resort to sources of surface water that are prone to pollution and serious health risks, including the transmission of waterborne diseases.

Additionally, Dumort's work in 1968 revealed that the study area was encompassed by two volcanic formations consisting of basalt and trachytes. Nzolang et al. [15] further established that the basement rocks comprised granites and gneiss of Pan-African origin. Moreover, Tematio [16] provided evidence that our study area was characterized by ferrallitic soils. Although these previous studies focused on petrology and pedology, no specific research was conducted on the hydrogeology of the Nord-Est part of the Menoua Division. To effectively exploit groundwater from subterranean aquifers, it is essential to gain preliminary knowledge of the hydrogeological and geophysical characteristics, such as depth, thickness, resistivity, and hydrodynamics of the aquifers. Therefore, our purpose was to employ 1D and 2D inversion in studying the underground aquifers of the Nord-Est part of the Menoua Division, with an aim of proposing a potential hydrogeological map for the area.

Within the scope of this study, geophysical methods, specifically 2D electrical resistivity tomography using the Schlumberger apparatus, were employed in conjunction with piezometric investigations. This approach enabled us to determine the resistivity of different formations, and to understand the distribution of resistivity of the subsurface rock in both depth and lateral dimensions. Additionally, it allowed us to determine the geometry of the underground aquifers and the various piezometric characteristics, which provide insights into the hydrodynamics of the aquifer system. These findings served as a valuable guide in the mapping of groundwater resources, facilitating a reliable assessment of the hydrogeological units within the subsurface.

2 Natural Setting

The study area, located on the southern flank of Mount Bamboutos, constitutes a section of the western highlands of Cameroon; it is between latitudes 5°32'0"N and 5°32'45"N, as well as between longitudes 10°7'0"E and 10°7'45"E in Figure 1a. The hydrography of the region is relatively underdeveloped and features a parallel network of water bodies originating from Mount Bamboutos. The digital elevation model in Figure 1b illustrates elevations ranging from 1530 to 1710 m. The landscape is characterized by hills and a valley formed as a result of tectonic and volcanic

activities. According to Morin in year 1988, five distinct morphologic levels could be observed and further divided into three divisions. The inferior surfaces, with altitudes ranging from 1530 to 1566 m, are primarily located in the southern part of the study zone. The intermediate surface elevations vary between 1566 and 1638 m, whereas the higher elevations, extending from 1638 to 1710 m, are mainly located in the northern sector of the investigated zone.

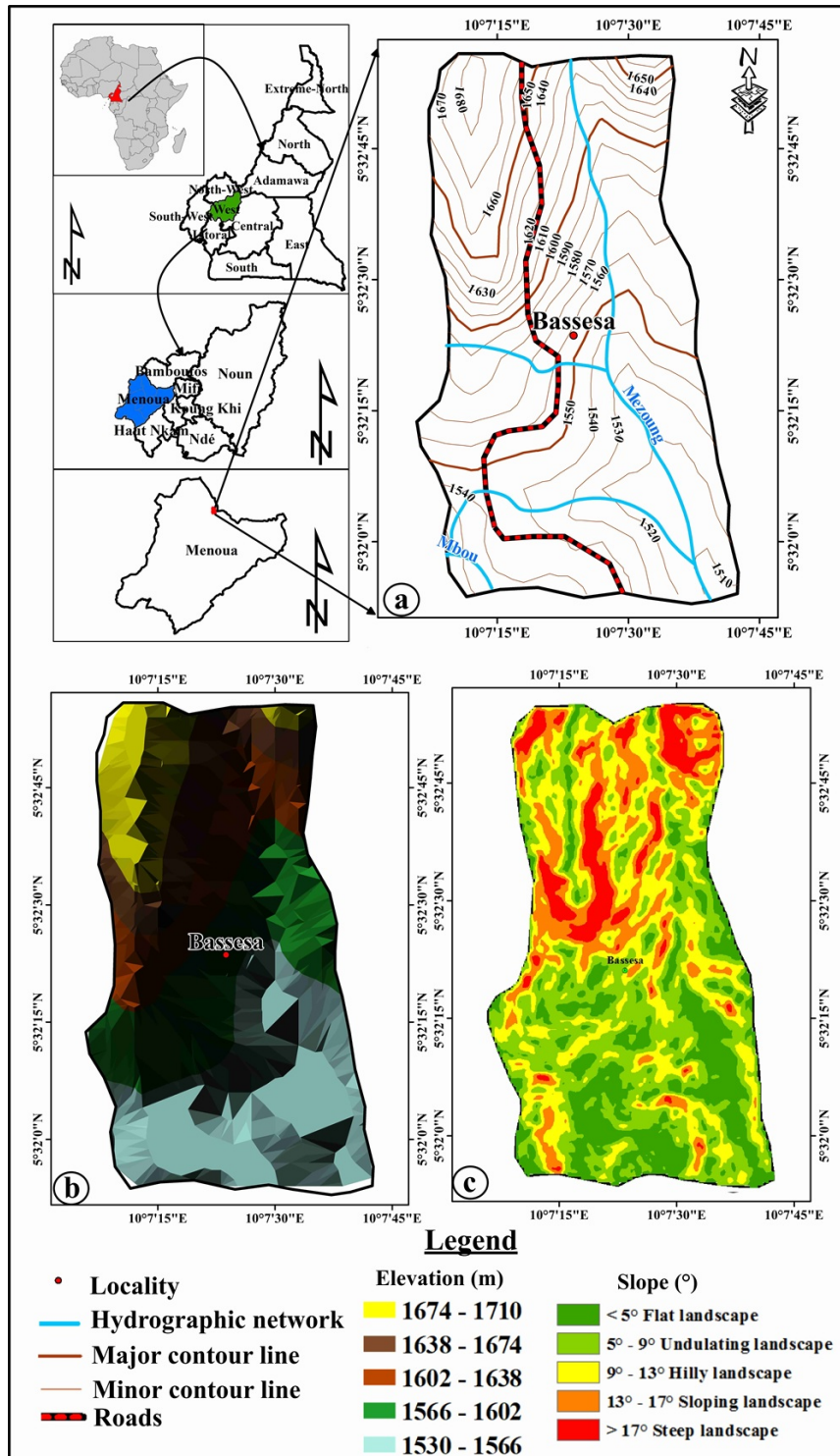


Figure 1. Natural setting: (a) Localisation map of the study zone; (b) Digital elevation model; (c) Slope map

The slope map in Figure 1c depicts five distinct classes of landscapes characterized by varied slopes. Smooth landscapes with slopes below 7° are mainly found in the southern part of the study area. Undulating landscapes with slopes ranging from 7° to 14°, and steep landscapes with slopes exceeding 14° are primarily observed in the northern part of the study area. To streamline this description and better align it with the hydrogeological objectives

in this study, we emphasize that gentle southern slopes favor infiltration and groundwater recharge, while steep northern slopes promote surface runoff, hence limiting infiltration and reducing groundwater accumulation. Thus, slope variations directly influence the spatial distribution of aquifers in the area.

The study area is composed of a basement of Precambrian granite and gneiss of Pan-African age [15, 17]; it is covered at the surface by volcanic formations as in Figure 2 and consists of: (i) Basalt, covering about 60% of the study zone, is a type of volcanic rock issued from rapid cooling of magma characterized by minerals such as plagioclase, pyroxene, and olivines; (ii) Trachyte, covering about 40% of the study zone, is an explosive volcanic rock rich in alkaline feldspars like sanidine, albite, and anorthose.

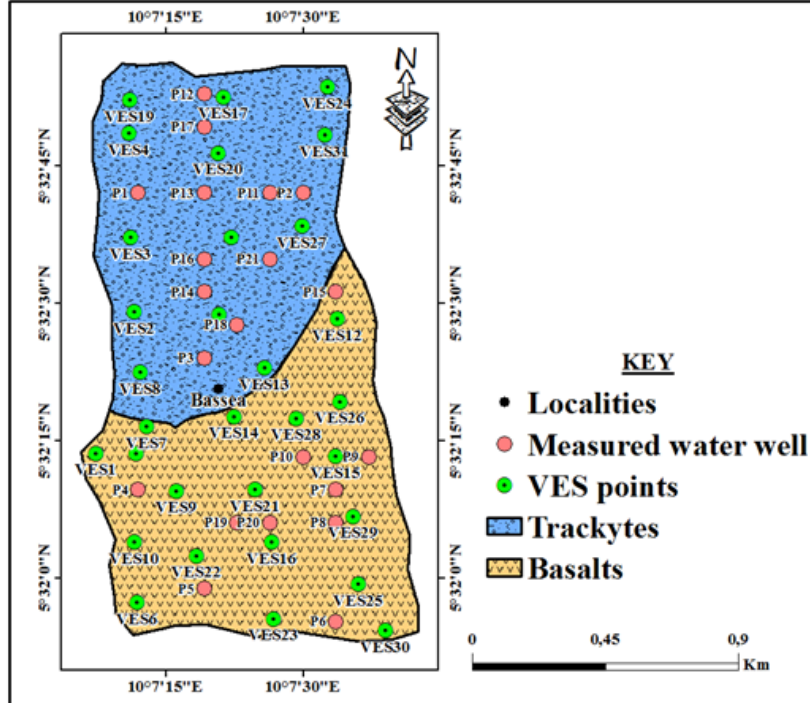


Figure 2. Spatial distribution of the Vertical Electrical Sounding (VES) and measured water wells on a Geologic map (extract from Dumort [18])

3 Methodology

This study adopted a dual-approach methodology comprising Vertical Electrical Sounding (VES) based on the Schlumberger array, and complementary hydrogeological investigations. For the component of the VES, fieldwork entailed a careful selection of appropriate locations to cater for the research objectives and geological considerations. The setup of equipment involved the placement of a resistivity meter and electrode arrays in accordance with the Schlumberger configuration. Data were collected by measuring resistivity at each VES point so as to ensure proper contact and stability of the electrodes. Essential field data, such as electrode spacing and observed geological features, were recorded. The collected VES data subsequently underwent laboratory processing, which involved utilization of suitable software and algorithms to process the data, generate iso-resistivity maps, and perform 1D and 2D geophysical inversions for interpretations. Eqs. (1) and (2) presented below summarize the necessary conversions required to obtain the apparent resistivity values.

$$\rho_a = \frac{k\Delta V}{I} \quad (1)$$

$$k = \frac{2\pi}{\frac{1}{AM} - \frac{1}{AN} - \frac{1}{BM} + \frac{1}{BN}} \quad (2)$$

In the following equations, I denotes the current intensity injected between electrodes A and B expressed in amperes, while ΔV corresponds to the potential difference measured between electrodes M and N in volts. The parameter k represents the geometric factor, which remains constant for a given electrode configuration and depends on the specific instrument used; it is expressed in meters (see Eq.(1)). ρ_a signifies the apparent resistivity

being analyzed and measured in Ohm meters; while A and B denote the current electrodes, M and N represent the measurement electrodes. These equations are not just provided as theoretical background; they constitute the basis for converting field measurements into hydrogeologically meaningful parameters. By establishing the correlation between resistivity and hydraulic properties like hydraulic conductivity, transmissivity, and porosity, these formulas help characterize aquifer thickness, permeability, and water-bearing capacity, which are central to assessing groundwater potential in the study area.

The production of iso-resistivity maps involved mapping the various $AB/2$ values distributed across the study area, ranging from $AB/2 = 1.5$ m to $AB/2 = 160$ m. Twenty-seven iso-resistivity maps were constructed for various depths of investigation corresponding to electrode spacings of $AB/2 = 1.5, 2, 3, 4, 5, 6, 7, 8, 10, 15, 25, 30, 35, 40, 50, 60, 70, 80, 100, 120, 140$, and 160 m.

In terms of the hydrogeological component, fieldwork primarily consisted of piezometry measurements aimed at determining groundwater levels and hydraulic head. Data regarding the flow directions of groundwater and other relevant hydrological parameters were collected, along with field observations of geological formations and structural features. The piezometric level (Np) of a well is determined using the following formula:

$$NP = A - (Zp - M) \quad (3)$$

where, A represents the altitude obtained through measurements by the Global Positioning System (GPS), Zp signifies the vertical distance between the soil surface and the water level in the well, and M denotes the well head. By utilizing the collected data, a piezometric map was created to visualize variations in groundwater levels. The interpretation of this map helped identify the flow patterns, hydraulic gradients, as well as recharge and discharge areas.

A total of 31 VES points, ranging from VES1 to VES31, and 21 wells from P1 to P21 were established; they were distributed across the two petrographic types of trachyte and basalt (Figure 2).

Additionally, hydraulic parameters such as hydraulic conductivity, transmissivity, and longitudinal conductance were calculated to gain insights into groundwater characteristics. Hydraulic conductivity K quantifies the ability of a porous medium to transmit fluids under a pressure gradient and is expressed in meters per day, as described in (4) [19, 20]. Porosity, representing the proportion of voids within a rock, is estimated using (5) [20]. Transmissivity Tr characterizes the rate of groundwater flow across the fully saturated thickness of an aquifer per unit of width under a hydraulic gradient. In this study, transmissivity was determined analytically using the relationship between transverse resistance S in Ω^{-1} in Eq. (6) and the link between transmissivity and longitudinal conductance in Eq. (7), following the assumption of a prism-shaped aquifer with unit cross-section and thickness h in meters [20, 21].

$$K = 386.40\rho^{-0.9383} \quad (4)$$

where, ρ denotes the resistivity of the aquifer in $\Omega \cdot \text{m}$, and K is the hydraulic conductivity in meters per day (see Eq. (4)).

$$\phi = 25.5 + 4.5 \ln K \quad (5)$$

where, K represents the hydraulic conductivity expressed in meters per day, and Φ denotes the porosity expressed as a percentage (see Eq. (5)) [20].

Eq. (6) defines the longitudinal conductance S as:

$$S = h/\rho a \quad (6)$$

where, h is the aquifer thickness in meters, ρ in $\Omega \cdot \text{m}$, and S is expressed in Ω^{-1} [21].

According to Eq. (7), transmissivity Tr is calculated as:

$$Tr = KS\rho \quad (7)$$

where, K is the hydraulic conductivity (m/day) and S is the longitudinal conductance (Ω^{-1}) [20, 21].

Finally, all collected data and interpretations were integrated to develop a comprehensive understanding of the hydrogeology of the study area.

4 Results and Discussion

4.1 Apparent ISO-Resistivity Maps

Out of the 27 resistivity maps generated, notable variability was observed in eight key depth levels: $AB/2 = 1.5$ m, 4 m, 10 m, 30 m, 60 m, 80 m, 120 m, and 160 m. These maps display different ranges of resistivity, spanning from 20.71 to 22 450.764 $\Omega \cdot \text{m}$, and can be categorized into three domains based on their apparent resistivity: low

resistivity for highly conductive areas, medium resistivity for less conductive areas, and high resistivity for resistant regions (as shown in Figure 3). At $AB/2 = 1.5$ m, three observable domains can be identified: a low resistivity domain ranging from 558.81 to 3834.79 $\Omega \cdot \text{m}$, mainly affecting the northwest and some traces in the central part of the study area; a medium resistivity domain from 3834.79 to 6898.04 $\Omega \cdot \text{m}$, impacting the southeast of the site; and a resistant domain from 6898.04 to 11 407.82 $\Omega \cdot \text{m}$, represented by two concentric resistivity anomaly zones in the northeast and southwest parts. At $AB/2 = 4$ m, the resistivity range varies from 201.39 to 24 034.43 $\Omega \cdot \text{m}$ and can be classified into three domains: A low resistivity domain from 201.39 to 5596.19 $\Omega \cdot \text{m}$, mainly affecting the northwest with some traces in the center; a medium resistivity domain from 5596.19 to 12 724.38 $\Omega \cdot \text{m}$, impacting the southern part; and a high resistivity domain from 12 724.38 to 24 034.43 $\Omega \cdot \text{m}$, located around the northeast. At $AB/2 = 10$ m, the resistivity variations are divided into three domains, fluctuating from 261.21 to 244 247.20 $\Omega \cdot \text{m}$. The low resistivity domain is more predominant, covering approximately 80% of the map from 261.21 to 6248.21 $\Omega \cdot \text{m}$, and mainly affects the south and northwest parts with some traces in the east. The moderate resistant area from 6248.21 to 17 723.16 $\Omega \cdot \text{m}$ covers around 5% of the map, with traces located in the southwest and north. The high resistivity domain from 17 723.16 to 34 427.20 $\Omega \cdot \text{m}$ covers 15% of the map and is situated in the northeast and southern tip of the site. At $AB/2 = 30$ m, the resistivity varies in three domains, ranging from 27.31 to 25 264.04 $\Omega \cdot \text{m}$. The map reveals that approximately 60% of the area is dominated by a low resistivity zone, with values ranging from 27.32 to 3973.51 $\Omega \cdot \text{m}$, mainly concentrated in the southwestern sector though minor extensions appear in the northern part. The medium resistivity zone, spanning 3973.52 to 13 295.31 $\Omega \cdot \text{m}$, covers roughly 15% of the surface and is characterized by a circular anomaly situated in the southeast, with some presence in the north. The high resistivity zone, ranging from 13 295.32 to 25 264.24 $\Omega \cdot \text{m}$, is primarily located in the northeastern sector. When the half-electrode spacing $AB/2AB/2AB/2$ equals 60 m in Figure 3e, the resistivity distribution is allocated to three main domains between 114.32 and 17 060.72 $\Omega \cdot \text{m}$. The low resistivity domain of 114.32–3142.50 $\Omega \cdot \text{m}$ maintains a similar spatial distribution, affecting around 60% of the area, predominantly in the southwest and sporadically in the north. The medium resistivity domain from 3142.50 to 9040.63 $\Omega \cdot \text{m}$ affects 20% of the map, mainly in the southeast with a circular anomaly and traces in the north. The resistant domain from 9040.63 to 17 060.72 $\Omega \cdot \text{m}$ impacts the northern edge of the study site. At $AB/2 = 80$ m, the resistivity is divided into three domains, ranging from 21.25 to 15 381.78 $\Omega \cdot \text{m}$. The low resistivity domain from 1.21 to 2493.15 $\Omega \cdot \text{m}$ affects the southwest with a few traces in the north. The medium resistivity domain from 2493.15 to 5821.54 $\Omega \cdot \text{m}$ is concentrated mainly in the southeast, whereas the high resistivity domain from 5821.45 to 15 381.78 $\Omega \cdot \text{m}$ is predominantly represented in the northwest and southeast. At $AB/2 = 120$ m in Figure 3g, the resistivity varies from 0 to 11 949.92 $\Omega \cdot \text{m}$ and can be categorized into three distinct domains. The first domain exhibits low resistivity values from 0 to 2028.03 $\Omega \cdot \text{m}$ and covers approximately 50% of the map, predominantly in the southwest with some traces in the northern region. The second domain corresponds to medium resistivity values from 2028.03 to 6214.72 $\Omega \cdot \text{m}$ and affects about 25% of the map, extending across the southeastern part with some traces in the north. The third domain, distinguished by high resistivity values ranging from 6214.72 to 11 949.92 $\Omega \cdot \text{m}$, occupies approximately 25% of the area in the map and includes a persistent anomaly located in the northern region. At a larger electrode spacing $AB/2 = 160AB/2 = 160AB/2 = 160$ m in Figure 3h, resistivity varies from 0 up to 9460.24 $\Omega \cdot \text{m}$ across the study area, and can be subdivided into three distinct domains. The first domain, corresponding to low resistivity values from 0 to 1531.67 $\Omega \cdot \text{m}$, encompasses about 40% of the area, mainly in the southwest with some scattered traces toward the north. The second domain represents medium resistivity values from 1531.69 to 4923.08 $\Omega \cdot \text{m}$, covering 30% of the map and extending from the southeast towards the west, with some traces in the north. Lastly, the third domain exhibits high resistivity values from 4923.08 to 9460.24 $\Omega \cdot \text{m}$, impacting 30% of the map, predominantly the northern part.

The current analysis highlighted low resistivity anomalies, generally corresponding to weathered alterites and fractured basaltic trachytes, which constitute the main aquifer-bearing formations. In contrast, high resistivity zones are associated with compact, unweathered volcanic rocks and granitic basement units that are less favorable for groundwater storage. This link between resistivity distribution and local lithological structures provided clearer evidence of the relationship between electrical signatures and aquifer occurrence in the study area.

These findings exhibited similarities with the research conducted by the study [22] in the Foto, Keleng, and Foréke regions. However, they differed from the results obtained by the study [11] in Ngoua (Dschang). In the Ngoua region of west Cameroon, iso-resistivity maps revealed both high and low resistivity domains at different depths of $AB/2$, i.e., 1.5 to 160 m. Notably, the central area exhibited an anomaly of average apparent resistivity from 20 to 7307.63 $\Omega \cdot \text{m}$, which coincided with eruptive rocks as described by the studies [23, 24]. When compared with these neighboring areas, the Menoua Division presented unique hydrogeological conditions, as aquifer thicknesses extended from 14.7 to 46.6 m and transmissivity values exceed 200 m^2/day in favorable zones. This comparison underscored the potential of the region to produce volcanic-alteritic aquifers in large amounts and featured the originality of the present study as well as its contribution to the strategies of regional groundwater development. The eruptive lithologies encountered in the area could possibly include large and fractured blocks of basaltic trachytes, which might constitute productive aquifers.

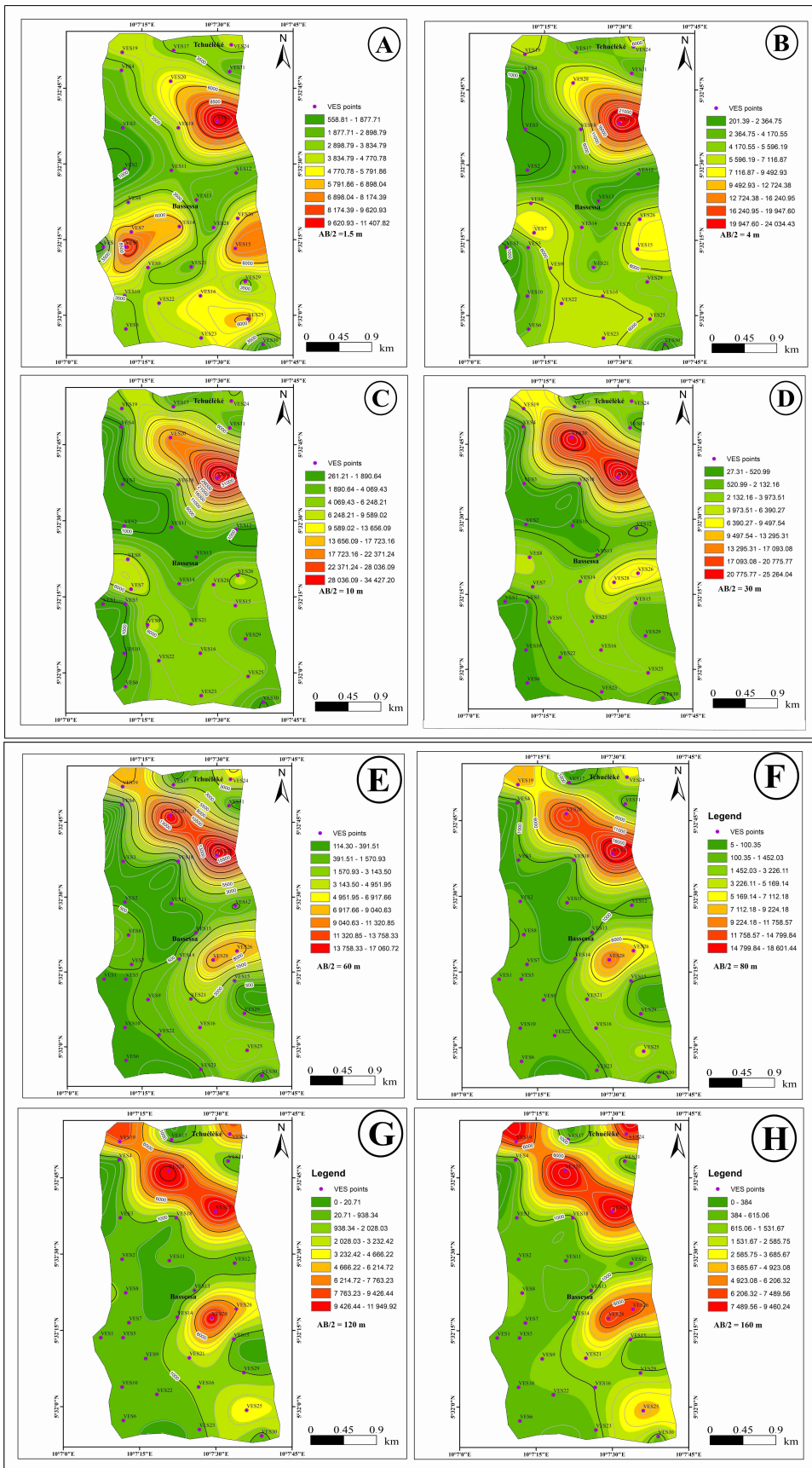


Figure 3. Apparent iso-resistivity maps: (a) For $AB/2 = 1.5$ m; (b) For $AB/2 = 4$ m; (c) For $AB/2 = 10$ m; (d) For $AB/2 = 30$ m; (e) For $AB/2 = 60$ m; (f) For $AB/2 = 80$ m; (g) For $AB/2 = 120$ m; (h) For $AB/2 = 160$ m

4.2 Inversion

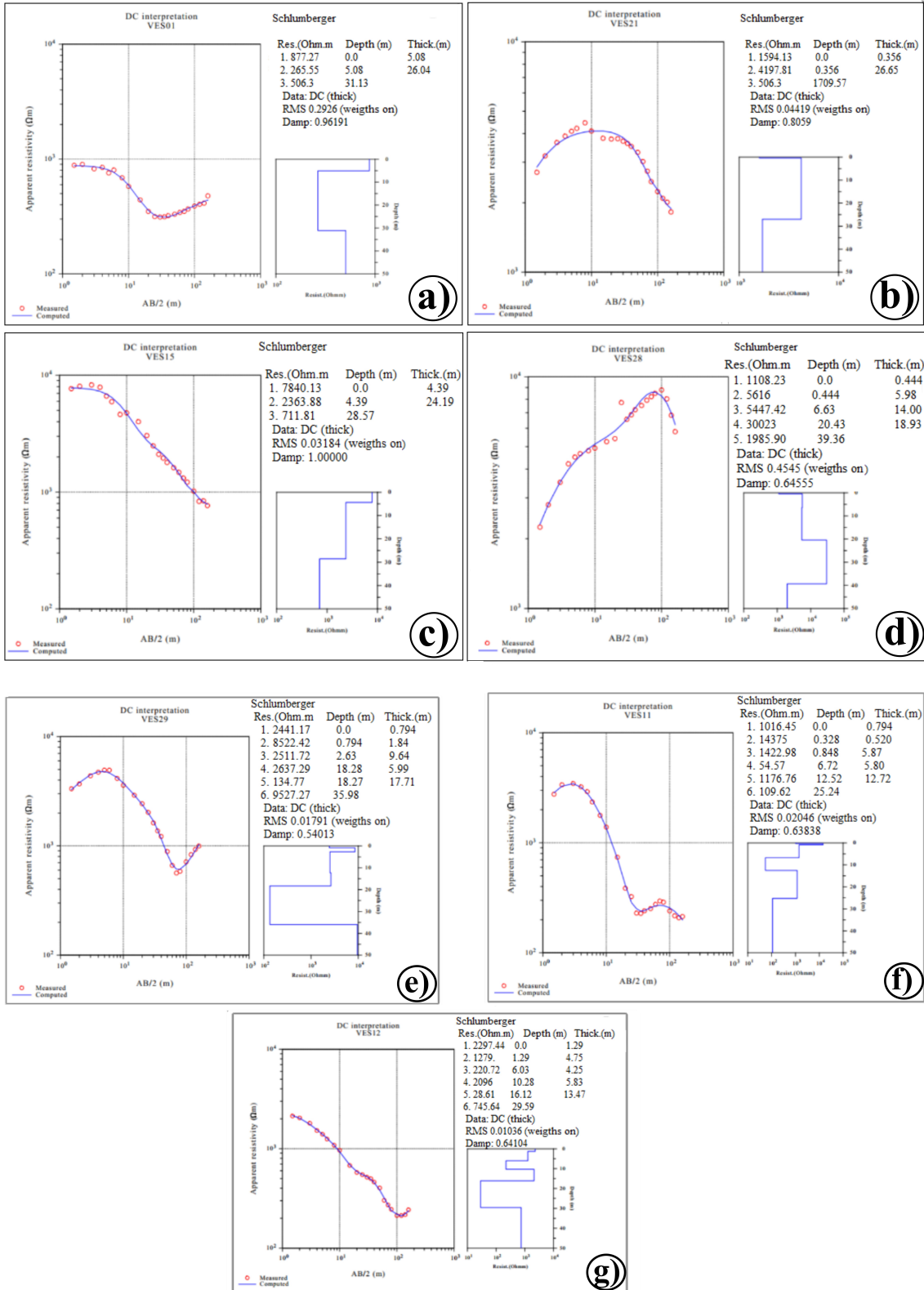


Figure 4. VES curve typology: (a) Type H; (b) Type K; (c) Type Q; (d) Type AK; (e) Type KH; (f) Type KHK; (g) Type QH

Through one-dimensional modeling analysis, seven distinct curve types H, K, Q, AK, KH, KHK, and QH were identified and mapped across the study area in Figure 4. True resistivity values range from 28.61 to 216,703 Ωm .

m, with an average of $5997.559 \Omega \cdot \text{m}$, while layer thicknesses vary between 0.228 and 46.64 m, averaging 7.549 m. These values exceed those reported by the studies [20, 25] for the Pouma quartzites, as they observed resistivity from 3 to $5800 \Omega \cdot \text{m}$ and thicknesses of the ground layers between 0.2 and 214.7 m. Their identified types of curves included QQH, QHK, QHA, QQQ, HAK, KHK, and QQ, as well as KH, KHA, QH, AKH, HK, H, AK, HA, A, and HKH.

These differences can be linked to lithological types. Metamorphic rocks in the two cases of study are at the same time linked to mineralogy, abundance of quartz feldspathic minerals, notably less abundant in the rocks in the volcanic cases of study.

The type H curve and those in association, such as KH and KHK, presented by the study [8] in the crystalline basement zone are those presenting a high hydrogeological potential because of the bottom of the boat which is the zone of very low resistivity. At the different corresponding depths, the bottoms of these boats indicate the presence of potential aquifers that can contain a fluid. The ascending branches of these curves indicate a change in lithological type from conductive to resistant ground. Types K, Q and AK curves, which are more represented in the centre and on the periphery of the study area, show the superposition of three layers of less and less resistant ground. For the study [10], these types of curves can show hydrogeological interest of the VES points considered, according to the nature of the terrain crossed.

The representations of Q, AK, and QH types in Figure 5a are relatively low. H and KH curves were in the central, western, eastern, and southern edges of the region while Q, AK, KHK, and QH types were scattered on both sides of the area. The dominant curve types throughout the study area were H and KH, each accounting for 25.806% of the total, followed by K and KHK at 19.355% and 12.903%, respectively (see Table 1 and Figure 5b).

Table 1. Proportion of different types of curves

Types of Curves	Frequencies	Corresponding VES Points	Percentage (%)
H	8	VES1, 2, 4, 5, 10, 13, 25, 30	25.806
K	6	VES8, 9, 20, 21, 23, 27	19.355
Q	2	VES15, 16	6.452
AK	1	VES28	3.226
KH	8	VES6, 7, 18, 19, 22, 24, 29, 31	25.806
KHK	4	VES11, 14, 17, 26	12.903
QH	2	VES3, 12	6.452

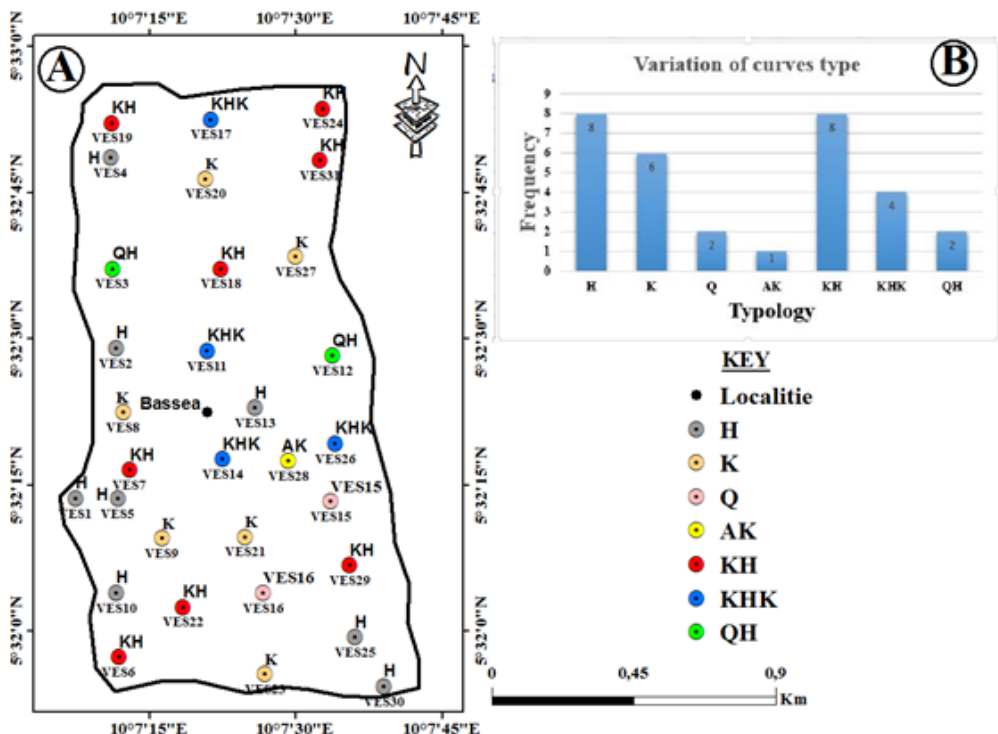


Figure 5. Distribution of different curve types: (a) Spatial distribution; (b) Histogram according to types of curves

For the lithological sections from 1D inversion, 18 logs were realized by excluding the points appearing more than once and following each VES point based on the different profile lines in Figure 6. For 2D inversions, four profiles were made. Profile P1 oriented N-S passed through the points of VES19, 4, 3, 3, 2, 8, 7, 5, 10, and 6. Profile P2 oriented N-S passed through VES31, 27, 12, 26, 15, 29, and 25. Profile P3 oriented NW-SE passed through the points of VES3, 11, 13, 28, and 15. Profile P4 oriented NE-SW passed through the points of VES12, 13, 14, 9, and 10.

The lithological sections were realized taking into account the different cross-sectional features of P1, P2, P3, and P4 with the corresponding VES points. This was guided by an abacus which consisted of electrical resistivity values for different geological materials presented by the study [24] and also by geologic observations of the study area in Figure 7.

The first layers represent the plant part, i.e., the organo—mineral. The second layers are weathering products from the weathering of the parent rocks. The other soil layers represent weathered or more or less sound rock levels. Different levels of potential aquifer zones are presented, either upstream on weathering products or downstream on weathered or more or less healthy rocks. These potential aquifers on alterite vary from 1.63 to 26 m and the levels of potential aquifers on fracture are above 26 m.

Lithological sections derived from 1D inversion are presented in Figure 7 for profiles P1 to P4. Profile P1 in Figure 8a, extending to a depth of 100 m, exhibited resistivity variations between 102 and 11 348 $\Omega \cdot m$. The upper, middle, and lower limits corresponded respectively to the depth intervals of 0–34 m, 34–64 m, and 64–100 m. From VES19 onwards, the profile showed a gradual arrangement of resistivities ranging from 768 to 11 348 $\Omega \cdot m$, influenced by geographic orientation. The remaining section displayed a circular pattern near the surface, with resistivities ranging from 102 to 291 $\Omega \cdot m$. The middle and lower zones, between VES3 and VES10, revealed a concave resistivity distribution fluctuating between 391 and 768 $\Omega \cdot m$, with notable peaks at VES4-3, VES5-6, and VES10.

Profile P2 in Figure 8b, also reaching 100 m deep, showed resistivities varying from 207 to 30 906 $\Omega \cdot m$. The upper, middle, and lower boundaries were spanning 0–34 m, 34–66 m, and 66–100 m, respectively. From VES31, 12, 15, and 29 onwards, the middle and lower sections exhibited resistivity values consistently between 207 and 864 $\Omega \cdot m$. However, at VES27 and 26, resistivities range from 15 114 to 30 906 $\Omega \cdot m$, with circular pockets near 30 906 $\Omega \cdot m$.

The 2D section of profile P3 in Figure 8c, extending to 90 m deep, displayed distinct boundaries at 30, 60, and 90 m. The overall structure consisted of separate vertical blocks with increasing resistivities from 212 to 12 552 $\Omega \cdot m$. Depending on the orientation, a low resistivity domain from 212 to 680 $\Omega \cdot m$ was observed between VES3, 11, and 13 within the middle depth interval.

Between VES13 and 15, the section appeared as a well-defined block with pockets of high resistivity, particularly between VES28 and 15, ranging from 3912 to 12 552 $\Omega \cdot m$, with a concentric band of 7007 $\Omega \cdot m$ encompassing all these limits.

Profile P4 in Figure 8d reached a depth of 80 m, with resistivity values ranging from 6.52 to 11 257 $\Omega \cdot m$. The upper zone from 0–27 m displayed resistivities between 1336 and 3882 $\Omega \cdot m$, including circular pockets around 1338 $\Omega \cdot m$ near VES12, 13, 14, 9, and 10. Between VES14 and 9, a stable resistivity of approximately 13 382 $\Omega \cdot m$ was maintained in the middle and lower sections. Notably, a concave resistivity zone ranging from 159 to 462 $\Omega \cdot m$ occurred at the lower limit between the VES and 13.

Maps of spatial variation in different resistivity ranges superimposed on the geological map of the sector, allows the realization of a geological model with resistivity sections from P1–P4 in Figure 8 based on field observations. From surface to base, initial soil sections mainly comprised weathered products, i.e., sandy, clayey-silty, clayey-sandy, and clayey soils with resistivities between 6.52 and 1073 $\Omega \cdot m$. The base of these sections showed a relatively intact and fractured substrate, with resistivities from 1073 to 30 906 $\Omega \cdot m$, resembling findings by the study [26] in the Kourwéogo area. Figures 8a–8c illustrate the aquifer levels as inferred from the resistivity variation map in Figure 8a, the 2D resistivity model in Figure 8b, and the geological model for profile P1.

Between the points of VES19 and VES4 along the N-S of the profile, the well individualized block arrangement of several ranges of resistivity allowed us to visualize several fractures which were structures for the circulation of water in hydrogeology in the basement zone. Overall, the profile showed five potential aquifer zones, with two on alterite located at about 19.5 m from VES19–VES7, and three potential aquifers on fractures located at about 85 m. These two types of aquifers developed respectively upstream on alteration products and altered rocks of basalt and trachytes, and downstream on more or less healthy fractured rocks. The knowledge of these different aquifers in 2D at greater depths helps visualize the depths achieved by 1D. Following this cross-section, this profile presents zones with variable hydrogeological potential of low, medium and high levels.

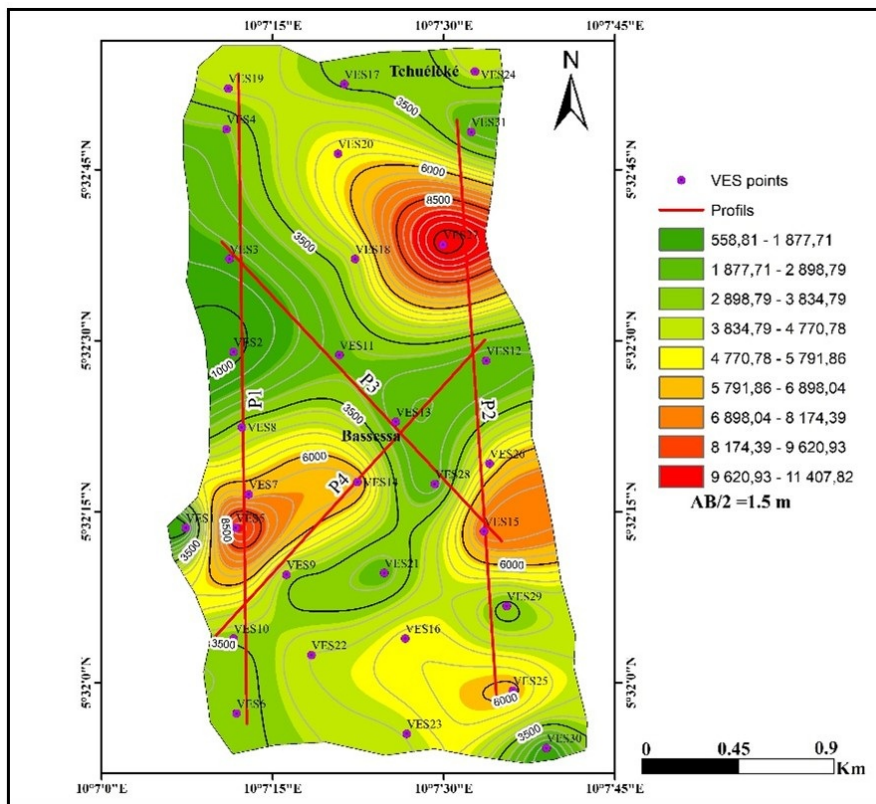


Figure 6. Presentation of different profile lines for 1D and 2D inversion

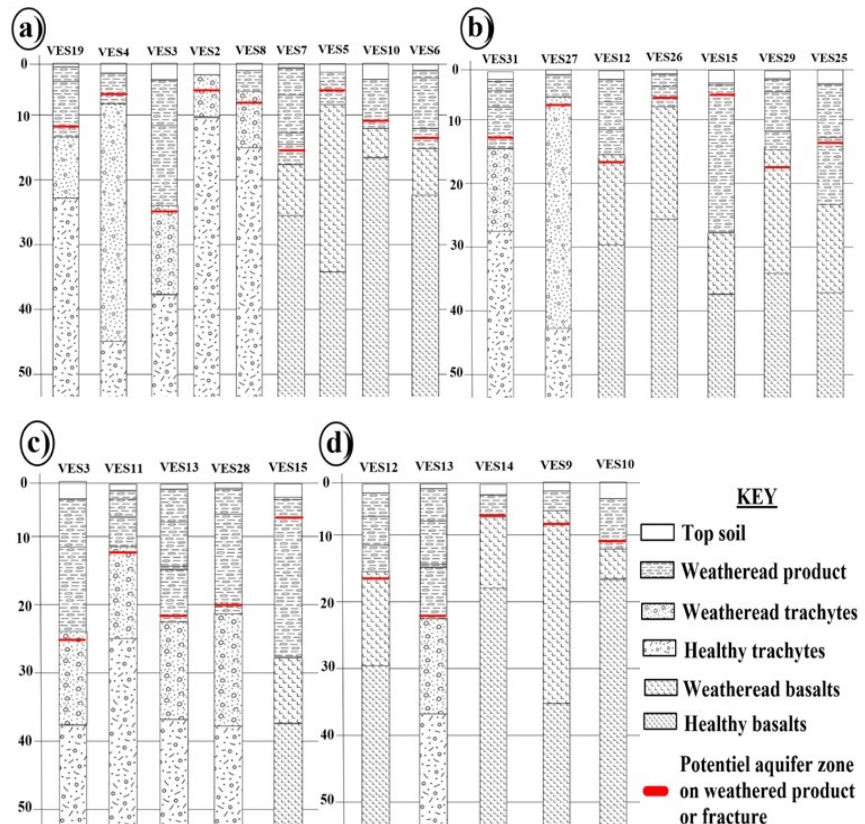


Figure 7. Lithological sections from 1D inversion: (a) Profile P1; (b) Profile P2; (c) Profile P3; (d) Profile P4

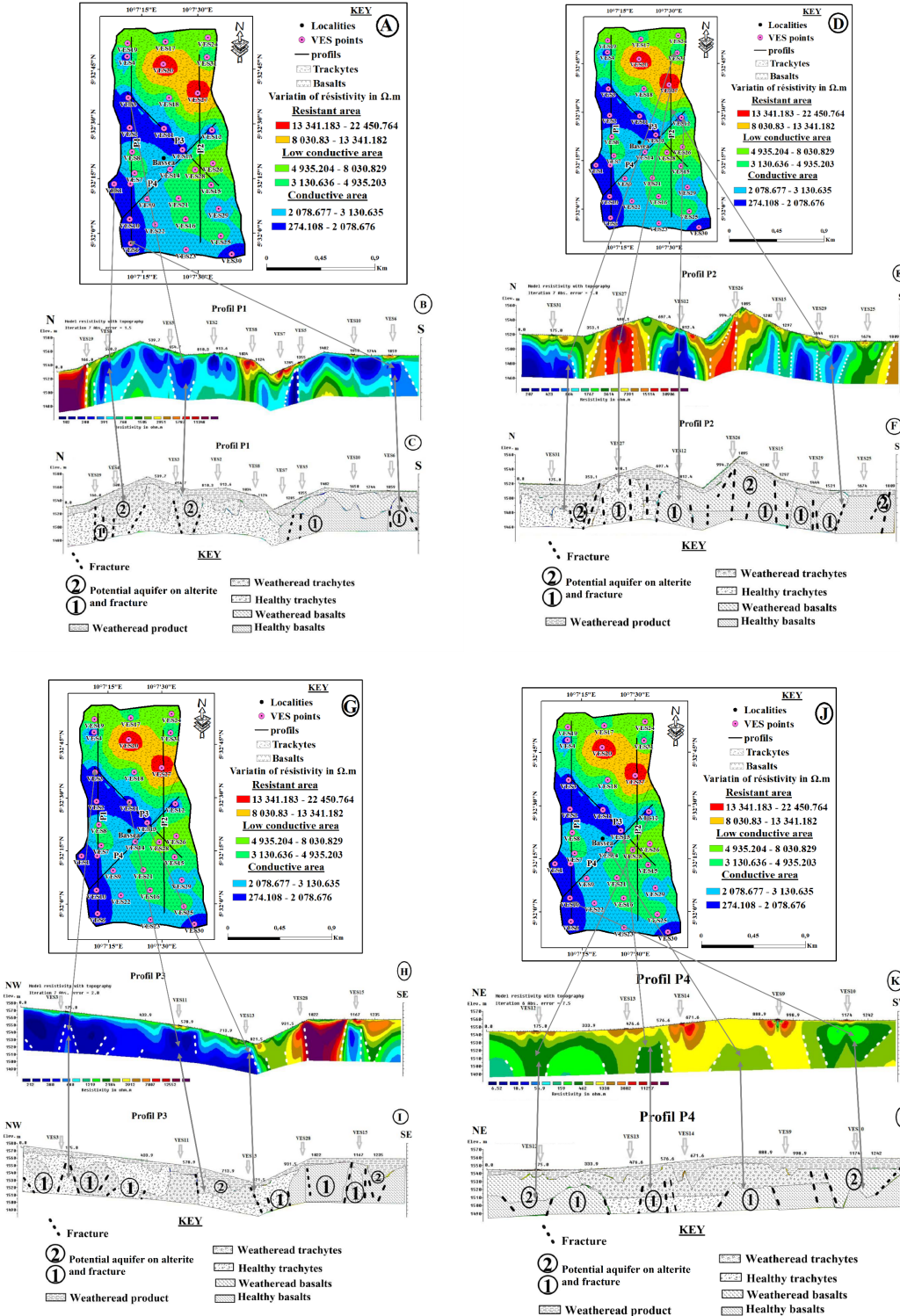


Figure 8. Representation of the anomalies related to the resistivity sections: (a) Spatial variations of different resistivity ranges; (b) Resistivity section of profile P1; (c) Geological model of the resistivity section of profile P1; (d) Resistivity section of profile P2; (e) Geological model of the resistivity section of profile P2; (f) Resistivity section of profile P3; (g) Geological model of the resistivity section of profile P3; (h) Resistivity section of profile P4; (i) Geological model of the resistivity section of profile P4; (j) Overlay of profile P4 resistivity section on the spatial resistivity variation map; (k) Hydrogeological model of profile P4 showing fracture and aquifer potential; (l) Depth distribution of alterite and fracture aquifers along profile P4

The lateral distribution of resistivity, arranged in blocks within the resistivity sections of profiles P2 and P3 in Figure 8d–8i, highlights fracture zones. This interpretation was supported by the abacus method from the study [24], other geological data, and field observations, which together informed the geological modeling. At approximately 3.5 m deep, moderate resistivity levels from 4935.20 to 8030.829 $\Omega \cdot \text{m}$ were recorded at VES31 and VES21 for P2, and at VES3 and VES13 for P3, all corresponding to weathering products such as clayey, sandy, and gravelly soils. Below 13.5 m, the blocky pattern of resistivities from 80.829 to 30 906 $\Omega \cdot \text{m}$ indicated fractured zones. This suggested the presence of a fracture-controlled aquifer at depth, which overrode the superficial alterite aquifer in Figures 8f–8i. Both profiles showed comparable zones with alterite aquifers deeper than 14 m and fractures extending from 14 to 86 m, as there were four developed fractures and four alterite zones.

Overall, profile P4 in Figures 8j–8k, overlaid on the resistivity variation map of the study area, revealed numerous fractures and zones with aquifer potential.

Beyond the first three meters, it showed products of alteration. At more than 3 m, it showed two potential aquifers on fracture and two others on alterite. The aquifers on alterite fluctuated around 14 and 23.5 m in depth and those on fracture up to 65 m in depth in Figure 8l.

The four profiles, P1–P4, provided comprehensive insights into the subsurface geology and electrical behavior along vertical and horizontal section lines, delineating different aquifer types. These findings, combined with the spatial resistivity distribution map, facilitated the identification of geophysical fractures in 2D inversion models that are conducive to aquifer formation in Figure 8.

4.3 Hydraulic Parameters

The spatial distribution of the calculated hydraulic parameters in Figure 9 reveals significant heterogeneity across the study area. The hydraulic conductivity (K) values range from 0.004 to 16.915 m/day. In Figure 9a, while transmissivity (Tr) varies between 0.017 and 227.841 m^2/day in Figure 9b, the longitudinal conductance (S) spans from 0.01 to 0.471 Ω^{-1} in Figure 9c, and the estimated porosity (ϕ) fluctuates from 0.736% to 12.524% in Figure 9d.

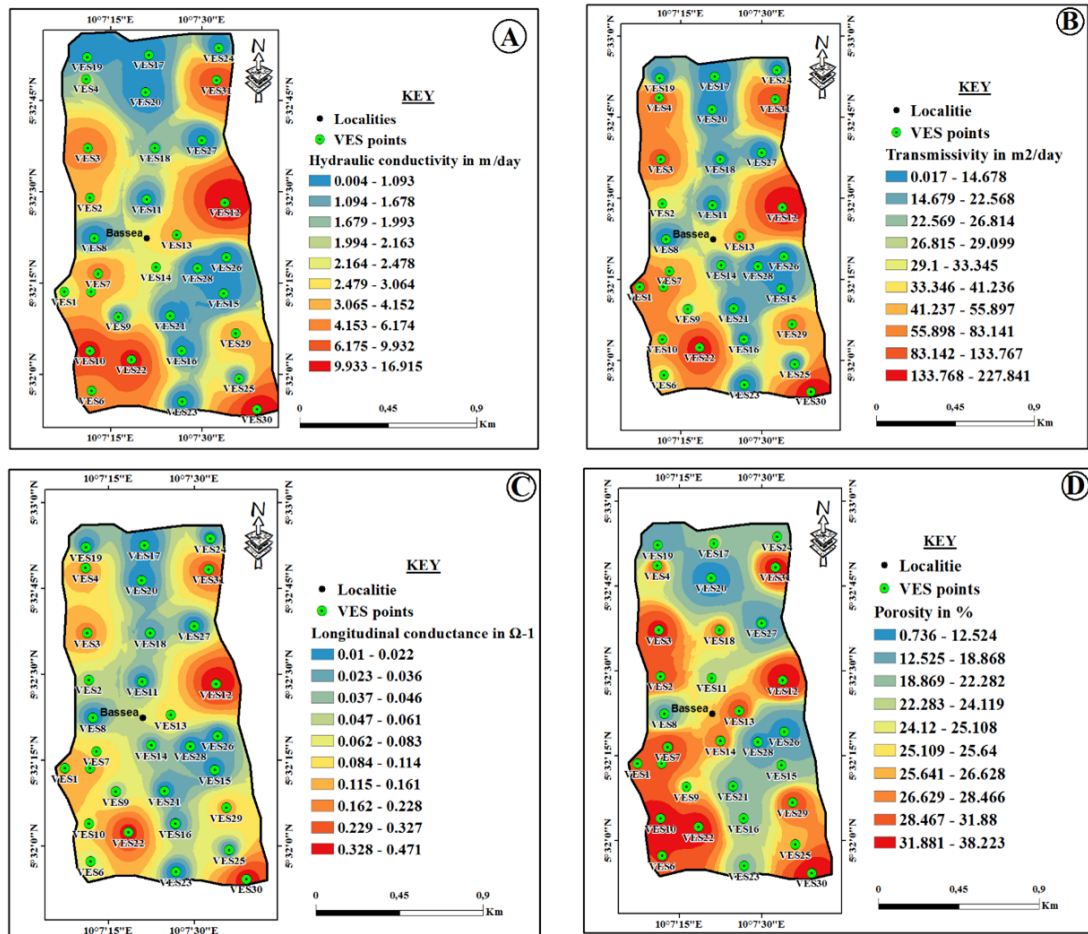


Figure 9. Spatial variations of the hydraulic parameters: (a) Hydraulic conductivity K ; (b) Transmissivity Tr ; (c) Longitudinal conductance S ; (d) Porosity ϕ

Higher values of K, Tr, and ϕ are mostly observed in the eastern, northeastern, and southwestern sectors of the area, reflecting ranges of 3.65 to 16.915 m/day, 41.237 to 227.841 m²/day, and 25.641% to 39.223%, respectively. In contrast, the northern and southeastern boundaries tend to exhibit lower hydraulic responses, with K varying between 0.004 and 3.065 m/day, Tr from 0.017 to 41.237 m²/day, and ϕ between 0.36% and 38.283%. Regarding longitudinal conductance, the central and northern zones generally present the lowest values (0.01 to 0.083 Ω^{-1}), whereas higher conductance (up to 0.471 Ω^{-1}) is more typical of the eastern and southwestern borders.

When compared with other regional studies, these values appear somewhat lower than those obtained in central Ondo State, Nigeria, where hydraulic conductivity ranged from 0.1382 to 48.121 m/day and transmissivity between 2.4705 and 221.3568 m²/day [27]. However, they are consistent with the ranges reported by the study [22], with K values between 0.004 and 44.852 m/day, porosity between 0.192% and 42.615%, S between 0.001 and 1.101 Ω^{-1} , and Tr from 0.019 to 504.023 m²/day.

Variations in hydraulic behavior are mainly influenced by subsurface lithology and degree of weathering. Zones with high K and Tr values are likely associated with fractured and permeable formations, such as weathered basalt, which tend to facilitate the movement of fluid. Conversely, low values are indicative of less permeable, possibly clay-rich or compacted layers which limit groundwater flow. This heterogeneity directly impacts aquifer development: productive boreholes are most likely to succeed in high K and Tr zones, while low-parameter areas pose risks of reduced yields or failure. Therefore, site-specific surveys remain essential before drilling and well siting strategies should prioritize the most permeable zones identified, while zones with lower parameters might require reinforcement measures such as deeper drilling or artificial recharge techniques to improve success rates [28].

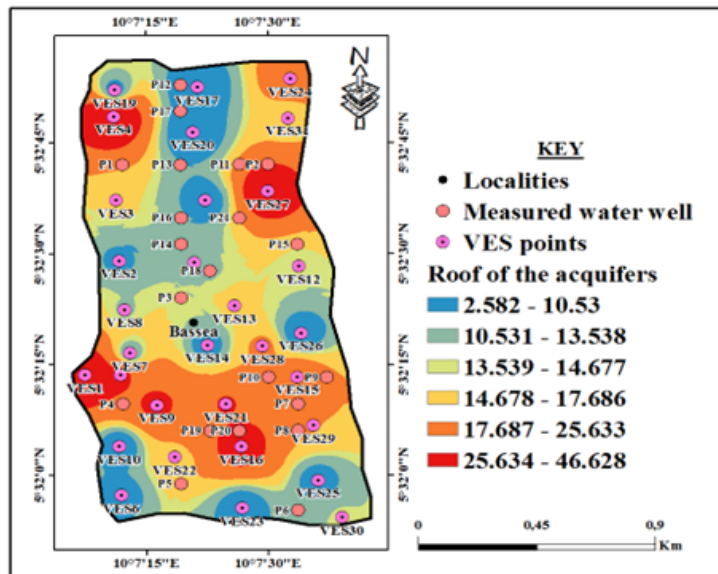


Figure 10. Map of the aquifer roof and thickness

By utilizing different aquifer levels and hydraulic parameters, a map is plotted in Figure 10 to tentatively depict the spatial distribution of aquifer thicknesses. These thicknesses range from 2.6 to 46.7 m and interestingly the values align closely with the findings of the study [11] in the Ngoua locality of Dschang, where aquifer thicknesses range from 2 to 74 m. Specifically, depths ranging from 2.6 to 13.5 m may correspond to the observed maximum level of wells in the field, whereas depths from 13.5 to 25.6 m correspond to aquifer levels in alterite formations. Besides, depths from 25.6 to 46.6 m indicate aquifer levels within more or less consolidated and fractured rocks. This classification differs somewhat from the findings of the study [29] in Dschang and its surrounding areas, where geophysical studies revealed the presence of two types of aquifers, including an alteration-based aquifer ranging from 21.5 to 28 m deep and a fractured aquifer from 28 to 40 m deep.

4.4 Piezometric

Based on the data from 21 wells, the piezometric map in Figure 11a together with the map showing the depth of water table in Figure 11b, provide key insights into groundwater dynamics. The piezometric map highlights distinct features, including piezometric hollows or depressions/recharge zones, and piezometric domes or discharge zones. Water levels range from 1520 to 1660 m and are divided into three main zones, i.e., the green domain of a high piezometric level zone between 1620 and 1660 m, the light-green domain of a moderate piezometric level zone between 1560 and 1620 m, and the blue domain of a low piezometric level zone between 1520 and 1560 m. The

overall pattern of current lines indicates a preferential northeast-southwest flow direction, except in the hollow zone where the current lines converge for groundwater, while surface water flow is oriented northeast-southeast.

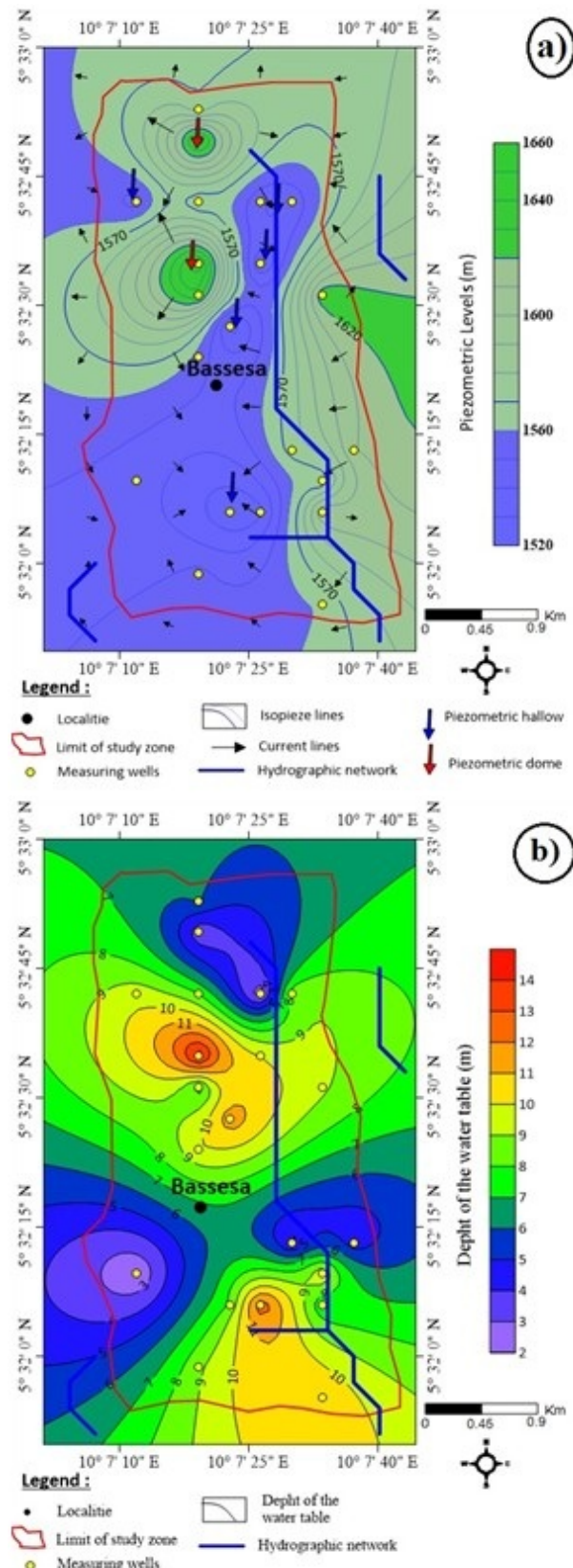


Figure 11. Flow directions and depth of the water table: (a) Spatial distribution of flow directions; (b) Spatial distribution of the depth of water table

The presence of four concentric hollows or depressions in the low piezometric level zone represents recharge zones, while the piezometric domes in the north signify areas of water table discharged through precipitation infiltration. The southwest and center of the study area, characterized by a depression zone, are favorable for capturing water as it accumulates from the piezometric domes. Consequently, the predominant direction of groundwater flow is from the northeast to the southwest, diverging primarily in the north and converging in the south, whereas surface water follows the northeast-southeast direction, aligning with the hydrographic network as a source of water table.

To highlight the practical significance of these dynamics, recharge mainly occurs through rainfall infiltration on higher elevation slopes and piezometric domes, where fractured volcanic rocks favor downward percolation. Discharge mechanisms, on the other hand, are concentrated in the southwestern depressions, where groundwater accumulates and can be sustainably extracted. This interaction between recharge and discharge zones explains the spatial variability of groundwater availability and provides essential guidance for selecting borehole sites with higher success rates.

4.5 Hydrogeological Potential Map of the Study Area

To determine the potential of groundwater development across the study zone, multiple datasets were integrated, including aquifer thickness, hydraulic parameters such as hydraulic conductivity, transmissivity, porosity, and longitudinal conductance, surface drainage systems, and geophysical indicators such as VES curve typologies and subsurface resistivity variations. The synthesis of these variables allowed classification of the region into three main categories of hydrogeological potential.

Located primarily in the northeastern and parts of the central zone, low potential areas are composed of about 10% of the territory; they are defined by limited aquifer thickness ranging from 2.6 to 13.5 m and by geoelectrical responses of types K and AK curves. These zones generally suggest poor groundwater productivity due to low permeability and minimal water retention capacity.

Moderate potential zones extend roughly over 40% of the study area, encompassing segments of the northeast, center, and southern portions. Aquifer layers in these zones range between 13.5 and 14.7 m in thickness, and the VES curves of types K and Q are predominant. These areas reflect medium hydrogeological characteristics, possibly associated with mixed lithological units of weathered materials and fractured rock zones which offer modest water yields.

High potential areas represent around 50% of the mapped zone and are primarily situated in the southwest, southeast, central, and portions of the northern regions. These areas are marked by thicker aquifer layers from 14.7 to 46.6 meters and associated with highly productive VES curves such as H, KH, KHK, and QH. The presence of these types of curves, in conjunction with high transmissivity and porosity values, suggests favorable geological structures conducive to groundwater storage and movement as in the examples of deep weathered profiles and fractured volcanic rocks.

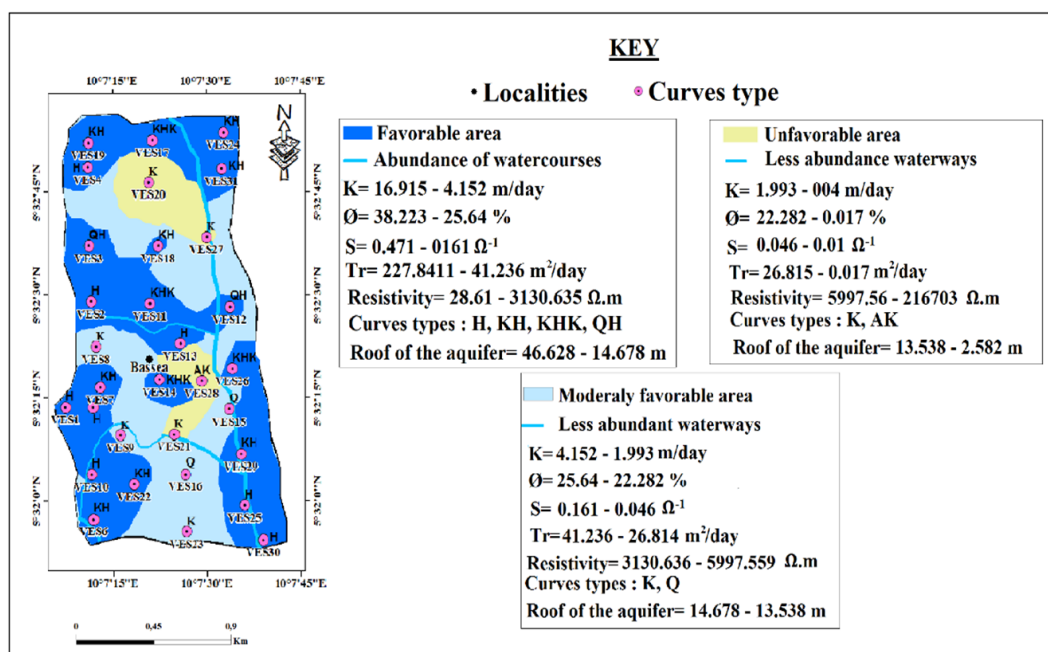


Figure 12. Hydrogeological map illustrating areas for groundwater exploitation

To ensure scientific validity and reproducibility, the classification thresholds are defined as follows: (i) Low potential zones correspond to aquifer thickness < 13.5 m and transmissivity $< 40 \text{ m}^2/\text{day}$; (ii) Moderate potential zones correspond to aquifer thickness between 13.5 and 14.7 m with transmissivity ranging from 40-80 m^2/day ; and (iii) High potential zones correspond to aquifer thickness > 14.7 m and transmissivity $> 80 \text{ m}^2/\text{day}$. These explicit criteria provide clear standards for categorizing groundwater potential and strengthen the applicability of the hydrogeological map as a decision-support tool.

The hydrogeological map in Figure 12 highlights areas with varying suitability for groundwater exploitation. This classification serves as a decision-support tool for targeted borehole drilling and hand-dug well development, especially in regions facing challenges from persistent water access.

5 Conclusions

The purpose of this work was to assess aquifers in the northeastern Menoua Division through 1D and 2D resistivity inversion techniques, thereby informing future water supply initiatives. Due to increasing population, overuse of surface water, and past project failures, reliance on groundwater resources has become critical and they deserve better preservation. The geophysical survey revealed three distinct resistivity domains: the resistant domain in the northeast, characterized by compacted soils and rocky formations upstream transitioning to more permeable rocks downstream; the central region with basaltic trachyte formations, indicating potential aquifers; and conductive zones dominated by alterites upstream and fractured rocks downstream. Aquifers in alterite zones vary in depth from 1.6 to 26 m, while those in fractured rocks extend beyond 26 m. Hydraulic parameters and the hydrogeological map indicate that aquifers in the southwest and southeast regions are more productive, with aquifer thicknesses ranging from 14.7 to 46.6 m, rendering these areas ideal for hand-dug wells and borehole installations. Additionally, piezometric studies suggested a groundwater flow from northeast to southwest with depression zones in the southwest and central parts, hence attesting to the suitability for water capture in the area. This study highlighted key aquifer characteristics and identified regions most suitable for projects about sustainable water supply, emphasizing the importance of groundwater resources to address local water challenges.

Looking ahead, future research should focus on integrating geophysical investigations with hydrochemical analyses to improve groundwater quality assessment, testing artificial recharge methods to enhance the sustainability of aquifers, and applying remote sensing for continuous monitoring of aquifer dynamics. Further efforts should be made to develop predictive models that minimize borehole failure rates and increase the efficiency of groundwater development, thereby ensuring the long-term resilience of water supply systems in the Menoua Division and other similar volcanic regions.

Data Availability

The data used to support the findings of this study are available from the corresponding author upon request.

Acknowledgements

We sincerely thank all individuals who contributed to the acquisition of geophysical and hydrogeological data, which was essential for the successful completion of this study.

Conflicts of Interest

The authors declare that they have no conflicts of interest.

References

- [1] Z. Kılıç, “The importance of water and conscious use of water,” *Int. J. Hydrol.*, vol. 4, no. 5, pp. 239–241, 2020. <https://doi.org/10.15406/ijh.2020.04.00250>
- [2] Y. Wada, M. Flörke, N. Hanasaki, S. Eisner, G. Fischer, S. Tramberend, and D. Wiberg, “Modeling global water use for the 21st century: The Water Futures and Solutions (WFaS) initiative and its approaches,” *Geosci. Model Dev.*, vol. 9, no. 1, pp. 175–222, 2016. <https://doi.org/10.5194/gmd-9-175-2016>
- [3] I. R. Akhtar, A. A. Mohd, M. H. Nazri, and A. B. Zainal, “Application of electrical resistivity method (ERM) in groundwater exploration,” *J. Phys.: Conf. Ser.*, vol. 995, no. 1, p. 012094, 2018. <https://doi.org/10.1088/1742-6596/995/1/012094>
- [4] J. Margat, “Exploitation et utilisation des eaux souterraines dans le monde,” UNESCO-BRGM, Tech. Rep., 2008.
- [5] S. Bulduc, M. Larocque, and G. Prichonnet, “Groundwater vulnerability in the Noir River watershed (Montérégie, Québec),” *Rev. Sci. Eau*, vol. 19, no. 2, pp. 87–99, 2006. <https://doi.org/10.7202/01324ar>
- [6] M. J. Wirmvem, T. Ohba, W. Y. Fantong, S. N. Ayonghe, J. Y. Suila, A. N. E. Asaah, G. Tanyileke, and J. V. Hell, “Hydrochemistry of shallow groundwater and surface water in the Ndop plain, North West Cameroon,” *African J. Environ. Sci. Technol.*, vol. 7, no. 6, pp. 518–530, 2013. <https://doi.org/10.5897/AJEST2013.1456>

- [7] J. Biémi, S. Deslandes, Q. H. J. Gwyn, and P. Jourda, "Influence des linéaments sur la productivité des forages dans le bassin versant de la Haute Marahoué (Côte d'ivoire): Apport de la télédétection et d'un système d'information à référence spatiale," *Télédétection Ressour.*, vol. 7, pp. 41–49, 1991.
- [8] Y. Koussoubé, S. Nakolendousse, P. Bazié, and A. N. Savadogo, "Typologie des courbes de sondages électriques verticaux pour la reconnaissance des formations superficielles et leur incidence en hydrogéologie du socle cristallin du Burkina Faso," *Sud Sci. Technol.*, vol. 10, pp. 26–32, 2003.
- [9] A. M. Kouassi, K. E. Ahoussi, K. A. Yao, W. E. J. A. Ourega, K. S. B. Yao, and J. L. Biémi, "Analyse de la productivité des aquifères fissurés de la région du N'Zi-Comoé (Centre-Est de la côte d'ivoire)," *LARHYSS J.*, vol. 2012, no. 10, pp. 57–74, 2012.
- [10] A. Boudoukha, "Identification des aquifères profonds par la prospection électrique. Application à l'Est algérien," *Sci. Technol. A*, vol. 28, pp. 47–52, 2008.
- [11] M. L. Kenzo Tongnang, "Apport de la géophysique à l'étude hydrogéologique du bassin versant de Ngoua, Ouest-Cameroun," Mémoire de Master, Université de Dschang, 2019.
- [12] E. A. Makem, "Geophysical and remote sensing contribution for groundwater exploration in the southwestern part of the Baleng Watershed: Implications for hand-dug wells and water boreholes," Mémoire de Master, Université de Dschang, 2020.
- [13] ECAM, "Deuxième enquête camerounaise auprès des ménages," International Household Survey Network, Enquête, 2001.
- [14] A. Nono, J. D. H. Likeng, H. Wabo, Y. G. Tabue, and S. Biaya, "Influence de la lithologie et des structures géologiques sur la qualité et la dynamique des eaux souterraines dans les hauts plateaux de l'Ouest-Cameroun," *Int. J. Biol. Chem. Sci.*, vol. 3, no. 2, pp. 218–239, 2009.
- [15] C. Nzolang, H. Kagami, J. P. Nzenti, and F. Holtz, "Geochemistry and preliminary Sr-Nd isotopic data on the Neoproterozoic granitoids from the Bantoum area, West Cameroon: Evidence for a derivation from a Paleoproterozoic to Archean crust," *Polar Geosci.*, vol. 16, pp. 196–226, 2003. <https://doi.org/10.15094/00003129>
- [16] P. Tematio, "Etude cartographique et pétrographique des sols ferralitiques et andosoliques dans les monts Bambouto (ouest-cameroun): Influence de la lithologie et des facteurs du milieu sur la nature et distribution des sols en région de montagne tropicale humide," Thèse de Doctorat, Université de Yaoundé I, 2005.
- [17] M. Kwekam, "Genèse et évolution des granitoïdes calco-alcalins au cours de la tectonique Pan-Africaine: Le cas des massifs syn-à tardi-tectoniques de l'Ouest-Cameroun (Région de Dschang et de Kékkem)," Thèse de Doctorat, Université de Yaoundé I, 2005.
- [18] J. C. Dumort, "Carte géologique de reconnaissance de la République fédérale du Cameroun, feuille N°: NB 32 SE 028," 1968.
- [19] P. C. Heigold, R. H. Gilkeson, K. Cartwright, and P. C. Reed, "Aquifer transmissivity from surficial electrical methods," *Ground Water*, vol. 17, no. 4, pp. 338–345, 1979. <https://doi.org/10.1111/j.1745-6584.1979.tb03326.x>
- [20] B. E. Oguama, J. C. Ibuot, and D. N. Obiora, "Geohydraulic study of aquifer characteristics in parts of Enugu North local government area of Enugu State using electrical resistivity soundings," *Appl. Water Sci.*, vol. 10, p. 120, 2020. <https://doi.org/10.1007/s13201-020-01206-2>
- [21] S. Niwas and D. C. Singhal, "Estimation of aquifer transmissivity from Dar-Zarrouk parameters in porous media," *Hydrology*, vol. 50, pp. 393–399, 1981. [https://doi.org/10.1016/0022-1694\(81\)90082-2](https://doi.org/10.1016/0022-1694(81)90082-2)
- [22] R. Talla Toteu, "Etude comparative des résistivités électriques des sols développés sur basalte, granite et gneiss des localités de Foto, Foreké et Kelen: Implication hydrogéologique," Mémoire de Master, Université de Dschang, 2020.
- [23] G. V. Palacky, "Resistivity characteristics of geological targets," *Electromagn. Methods Appl. Geophys.*, vol. 1, pp. 53–129, 1987. <https://doi.org/10.1190/1.9781560802631.ch3>
- [24] L. Marescot, "Introduction à l'imagerie électrique du sous-sol," *Bull. Soc.*, p. 23, 2006.
- [25] P. N. Jude, K. J. Victor, W. Pierre, N. O. Anoh, M. E. Abasoh, D. M. M. Rosvelt, and T. C. Tabod, "Petrographic, morpho-structural and geophysical study of the quartzite deposit in the central part of Pouma, Littoral-Cameroun," *Results Geophys. Sci.*, vol. 7, p. 100019, 2021. <https://doi.org/10.1016/j.ringps.2021.100019>
- [26] P. K. Wendgouda, "Caractérisation hydrogéologique d'un aquifère en milieu de socle fracturé: Cas de la province du Kourwéogo," Mémoire de Master, Institut National d'Ingénieur de l'Eau et de l'Environnement, 2012.
- [27] O. Falowo, O. O. Olayemi, and S. D. Abayomi, "Groundwater resource assessment by hydraulic properties determination for sustainable planning and development in central part of Ondo State, Nigeria," *Environ. Earth Sci. Res. J.*, vol. 7, no. 1, pp. 1–8, 2020.

- [28] T. S. Tchomtchoua, “Apport de la géophysique à la caractérisation des eaux souterraines: Cas d'une localité de Batie, Ouest-Cameroun,” Mémoire de Master, Université de Dschang, 2020.
- [29] S. N. Masso Fowe, “Interaction eau-roche dans les hauts plateaux de l’Ouest-Cameroun: Cas de la ville de Dschang et ses environs,” Mémoire de Master, Université de Dschang, 2012.